nature electronics

Supplementary information

https://doi.org/10.1038/s41928-025-01560-6

Flexible kirigami microelectrode arrays for neuronal activity recordings in non-human primate brains

In the format provided by the authors and unedited

This PDF file includes:

Supplementary methods

Supplementary figures 1-12

Supplementary methods

Device structure characterizations. Optical image in **Fig. 1a** were obtained by the automated acquisition and stitching of an Olympus LEXT OLS4000 laser scanning confocal microscope (Olympus Corporation). Scanning electron microscopy (SEM) and cross-sectional SEM images in Fig. 1d-g were collected using a Nova Nanolab 200 FIB/SEM dual beam system (FEI Corp.).

Immunohistochemistry and tissue imaging. All animal procedures on mice were approved by the Animal Care and Use Committee of the National Center for Nanoscience and Technology, China. Male C57BL/6 mice (Vital River Laboratory Animal Technology Co. Ltd.) were used for immunohistochemical analysis. The mice were 8 weeks old and weighed 20-30 g at the time of *ki*-MEA implantation.

Immunohistological analysis were carried out at 8- or 10-weeks post implantation. The mice were anesthetized by intraperitoneal injection of 0.3% Zoletil 50 and 0.3% Xylazine Hydrochloride, and transcardially perfused with 1X PBS and 4% paraformaldehyde. The brain was removed and incubated in 4% paraformaldehyde overnight for post fixation. The brain was embedded in OTC and frozen at -20°C for 2 h before being sectioned into 30-μm-thick slices (Leica Biosystems). The brain was sliced perpendicular to the implanted filaments. The brain slices were incubated in 0.3% Triton X-100 for 15 min and 3% bull serum albumin (BSA) for 1 h at room temperature. The slices were transferred into primary antibody (1:500 dilution, ABN78 for neurons, Millipore and 1:1000 dilution, PA110004 for astrocyte, Invitrogen) overnight at 4°C. After being rinsed with 1X PBS, the slices were incubated in fluorophore-conjugated antibody for 2 h. Goat anti-rabbit immunoglobulin G (IgG) [heavy and light chains (H + L)] secondary antibody 488 (1:1000 dilution, A-11008, Thermo Scientific) and goat anti-chicken IgY (HL) Alexa-633 (1:1000, M213701S, Abmart) were used for neuron and astrocyte staining. After being rinsed with 1X PBS, the slices were mounted on glass slides. Fluoromonut G was used to protect the fluorophores from quenching. Confocal fluorescent images were acquired on a Zeiss LSM710 confocal microscope (Carl Zeiss X-ray Microscopy Inc.) using 488-nm laser as the excitation source for Alexa Fluor 488 and 633-nm laser as the excitation source for Alexa Fluor 633.

Supplementary figures

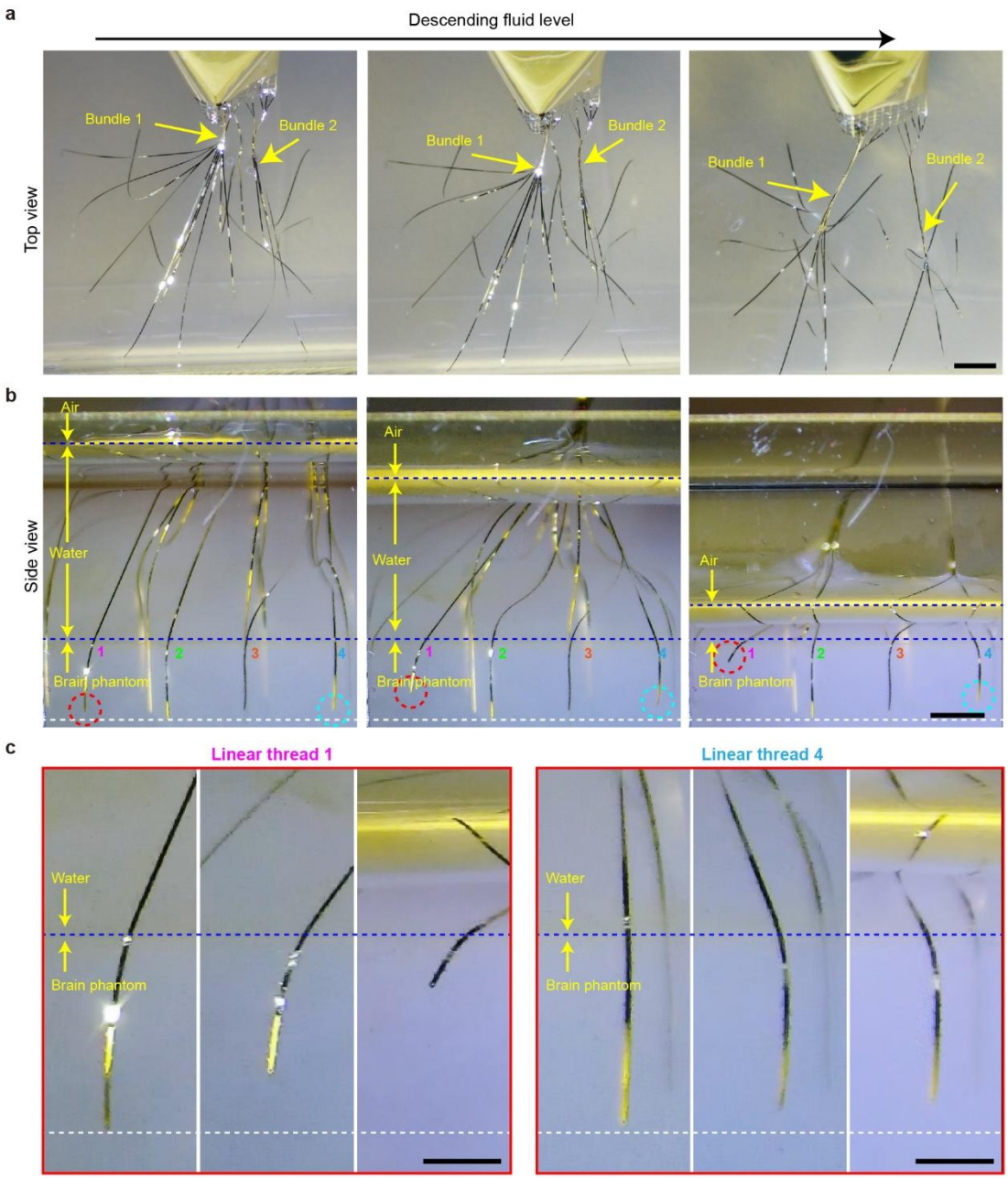

Supplementary Fig. 1. Capillary force induced bundling and retraction of linear threads. a, Top views of a 4X4 linear thread array after implantation into an agarose brain phantom. In the presence of fluid dynamics, capillary force pulls the linear threads together to form bundles, as highlighted by the yellow arrows. Scale bar, 2 mm. **b**, Side views of implanted linear threads under fluctuations of fluid levels. Capillary force-induced bundling causes upward retractions of implanted linear threads from the brain phantom, as highlighted by the red and blue dashed cycles. Scale bars, 2 mm **c**, Enlarged views showing the retraction of two example linear threads. Scale bars, 1 mm.

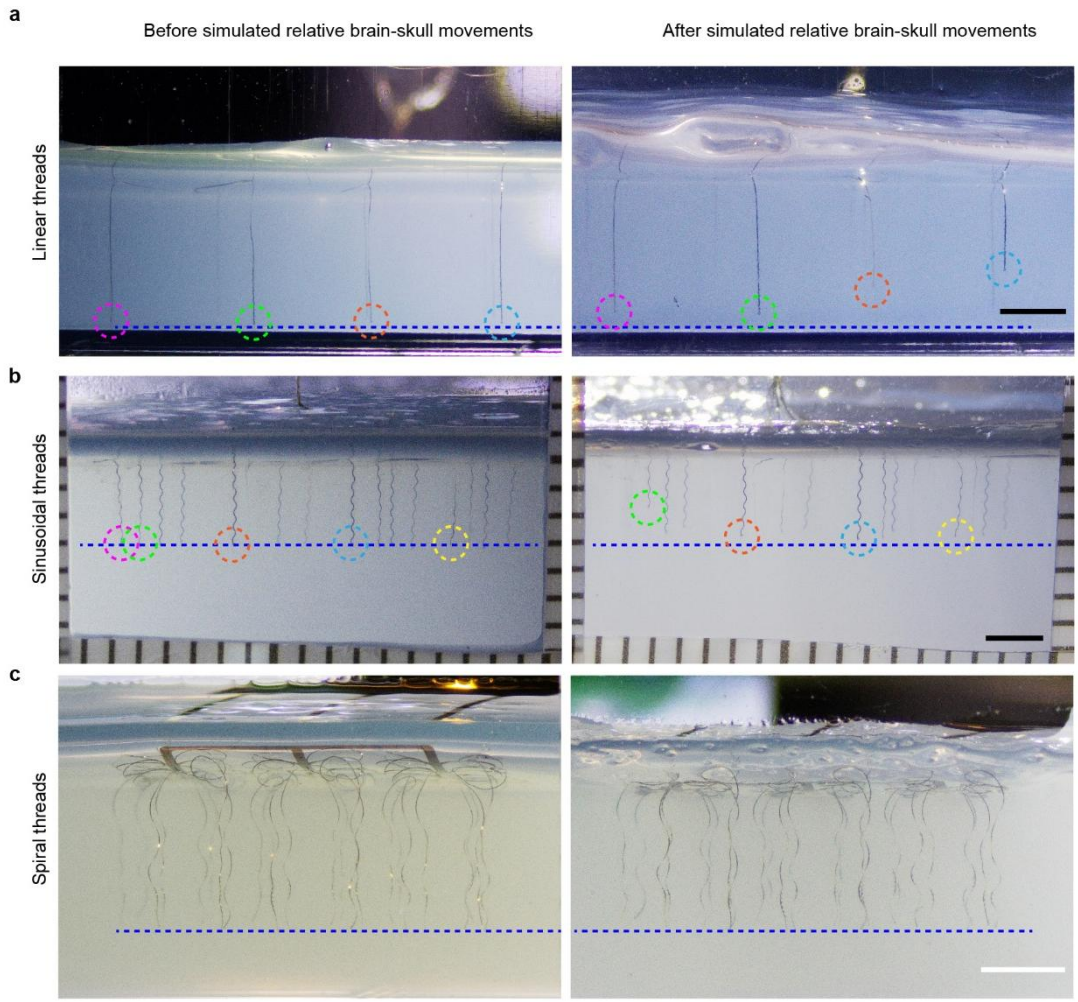

Supplementary Fig. 2. Simulated movements between the brain and skull. Arrays of linear threads (**a**), sinusoidal threads (**b**), and spiral threads (**c**) were implanted into agarose brain phantoms. The front bases of the arrays were fixed, while the brain phantoms were subjected to reciprocating motions of 500 μm at 2.5 Hz for 60 min. The distal ends of several linear and sinusoidal threads retracted from the brain phantom during the relative movements between the brain phantom and the fixed front base of the device because of their lack or limited of stretchability. The distal ends of the sinusoidal threads were retracted too. One of sinusoidal threads was even completely leaving the brain phantoms. On the other hand, the stretching of the floating turns of the spiral threads on the surface effectively accommodated the relative movements between the brain phantom and the fixed front base of the device. As a result, there was no dislocation of the distal ends of the implanted spiral threads inside the brain phantom. Scale bars, 2 mm.

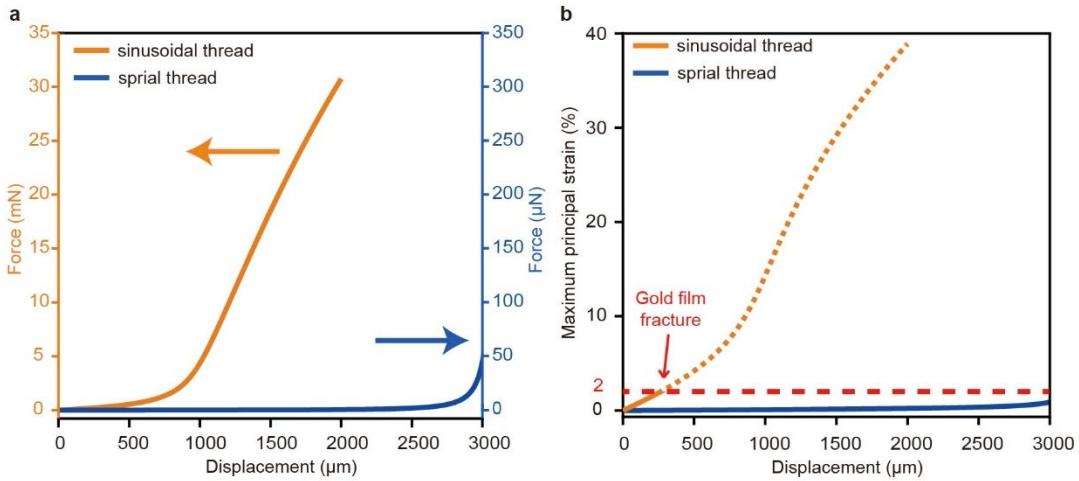

Supplementary Fig. 3. FEA simulation of spiral and sinusoidal threads upon stretching. a, Force–displacement curve of both spiral and sinusoidal threads under tensile loading. One end of each thread is fixed, while the other end is subjected to a tensile force to induce stretching displacement. The tensile force required to stretch a sinusoidal thread by 2 mm is 31 mN. In contrast, the tensile force required to stretch a spiral thread by 3 mm is only 46 μN. **b,** Maximum principal strain–displacement curve of both spiral and sinusoidal threads under tensile loading. Red dashed line highlights the fracture strain of thin gold films. The maximum principal strain on the sinusoidal thread reaches 2% with only 280 μm of stretching displacement. When the sinusoidal thread is stretched to 2 mm displacement, the maximum strain on the sinusoidal thread reaches 38%, far exceeding the fracture limit of the thin gold film. In contrast, the maximum strain of the spiral thread is 0.9% when stretched by 3 mm.

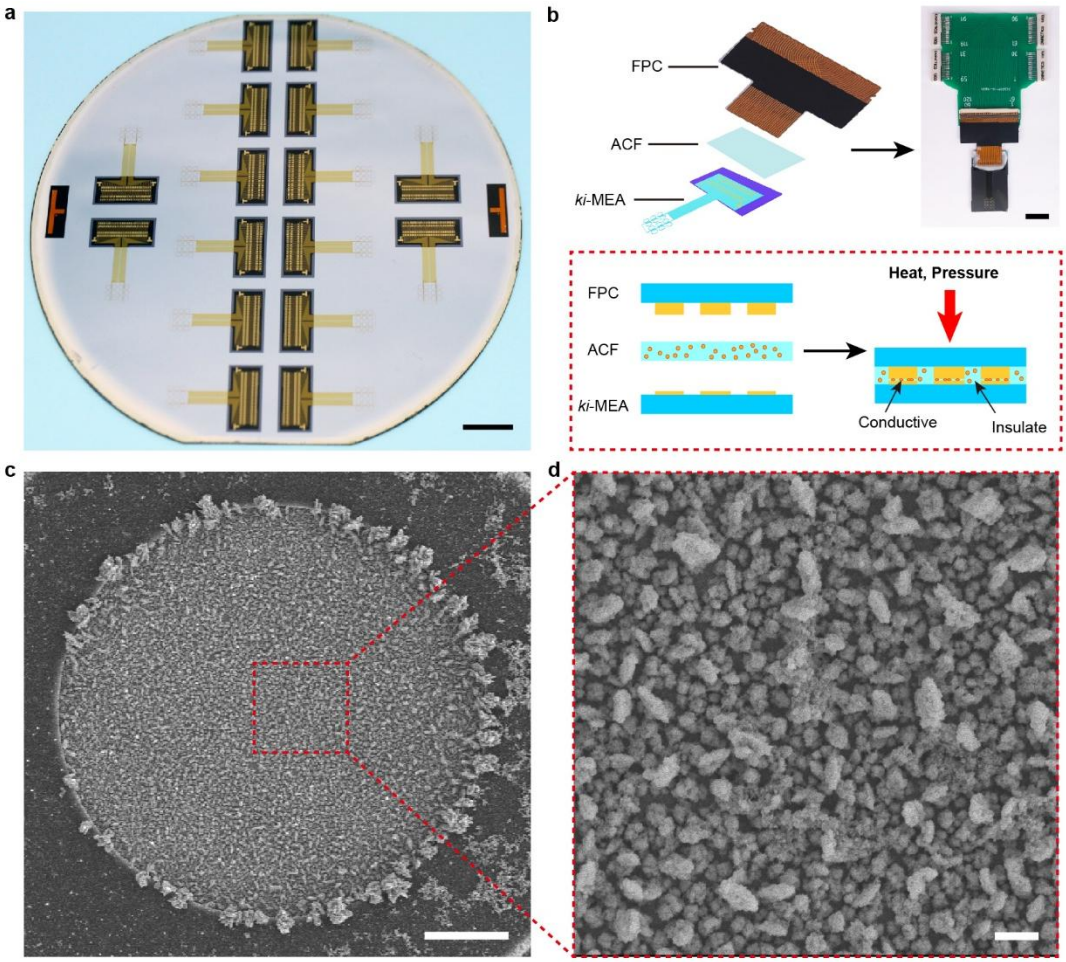

Supplementary Fig. 4. Bonding, electrical connections, and electrochemical deposition of platinum black of *ki*-MEA. a, As-fabricated *ki*-MEAs on a 4-inch silicon wafer. Scale bar, 1 cm. **b**, Flip-chip bonding of a *ki*-MEA to a FPC using an anisotropic conductive film (ACF). Inset, Photo of a *ki*-MEA probe connected to a PCB with four 36-pin Omnetics connectors. Scale bar, 5 mm. **c, d,** Scanning electron micrographs of a microelectrode site after platinum black coating process. Scale bars, 4 μm in **c** and 400 nm in **d**.

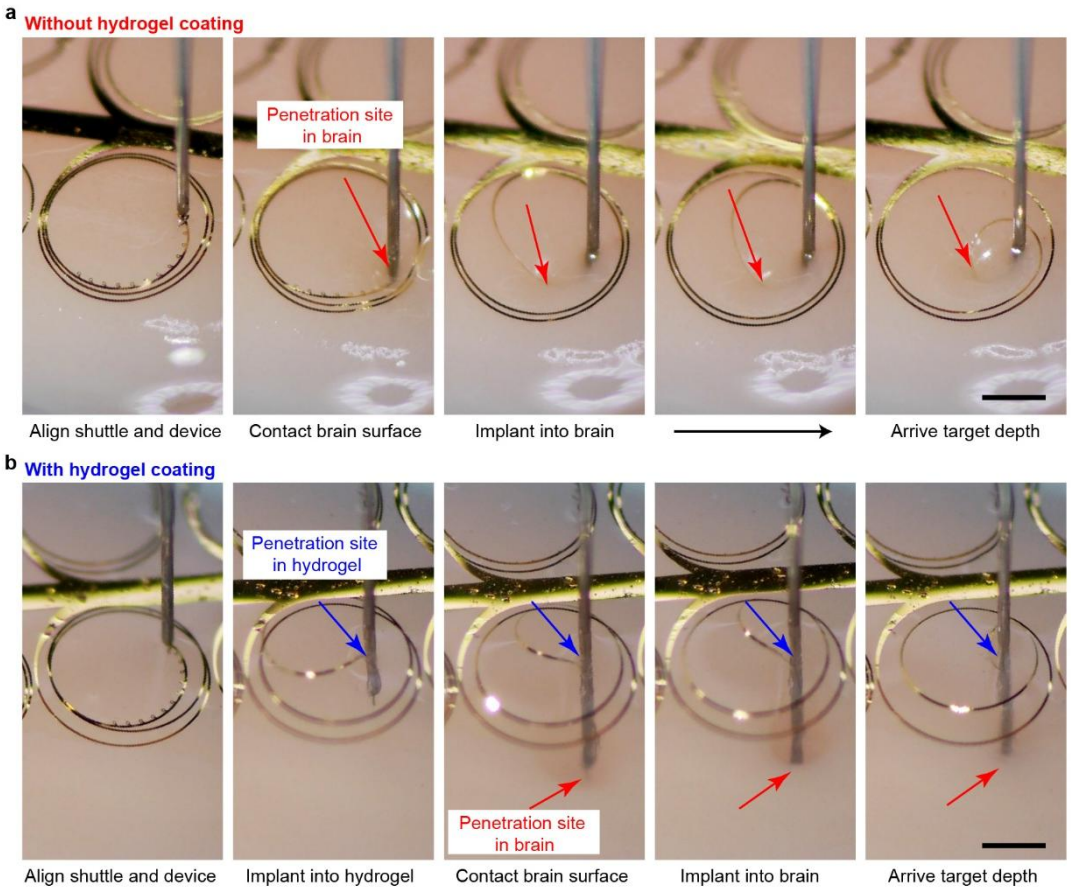

71

72 **Supplementary Fig. 5. Implantation without (top) and with (bottom) alginate hydrogel coating.**
73 Red and blue arrows highlight the penetration sites in the brain and hydrogel, respectively. Scale bars
74 500 μm.

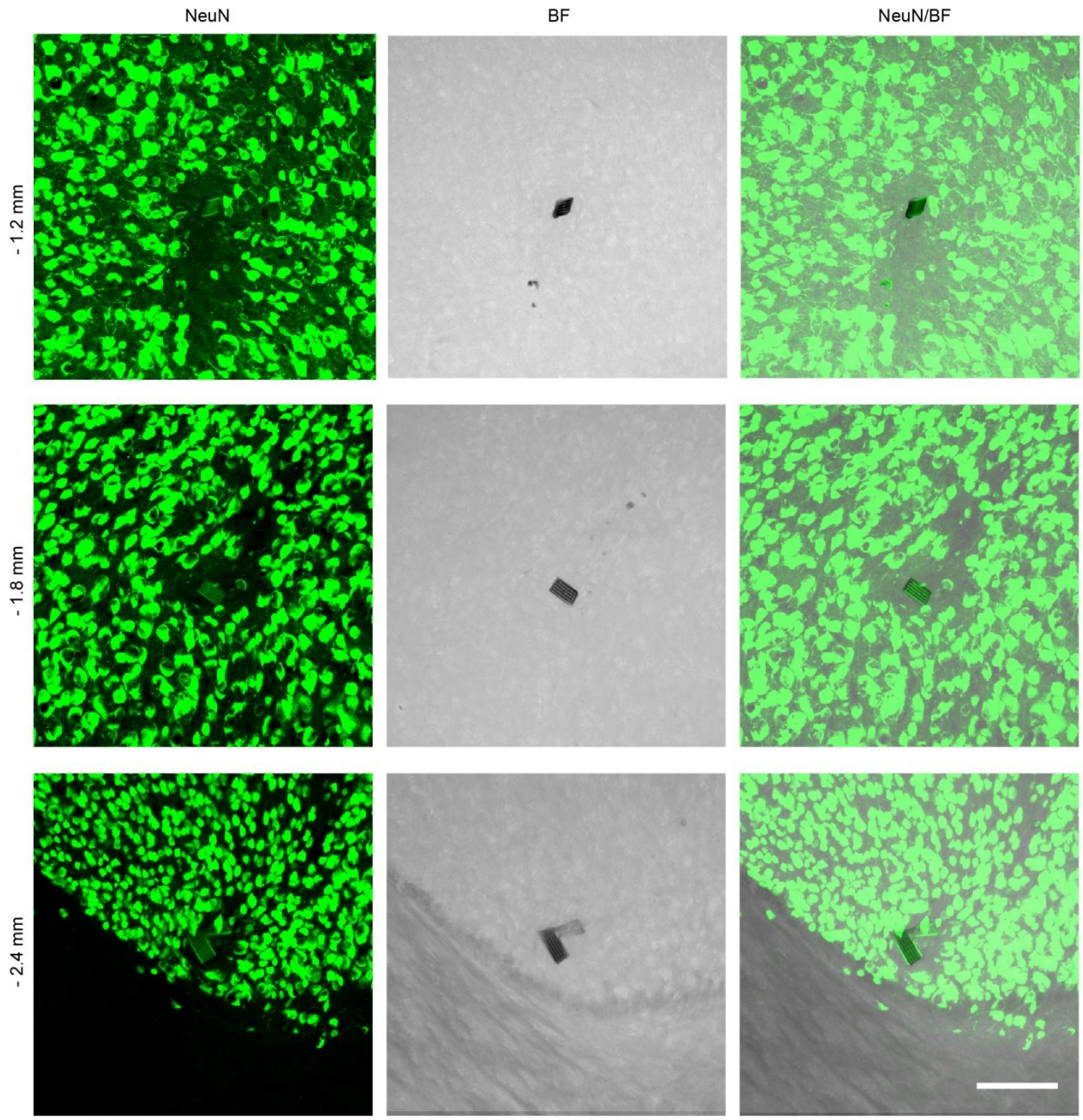

Supplementary Fig. 6. Depth-dependent immunohistological analysis of a chronically implanted *ki*-MEA. Horizontal mouse brain slices of 30 µm in thickness were prepared at 10 weeks post implantation and labeled for neurons (NeuN, green). The spiral thread can be seen in the bright field (BF) images. The three example brain slices (from top to bottom) were 1.2 mm, 1.8 mm, and 2.4 mm deep from the brain surface, respectively. Scale bar, 100 µm.

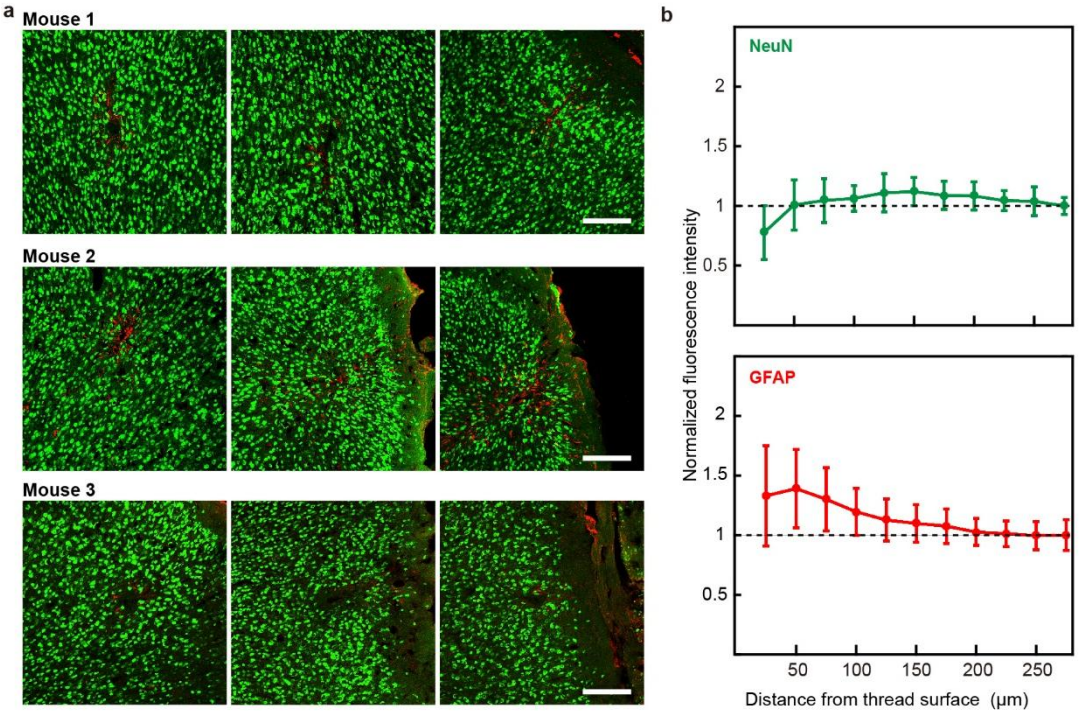

Supplementary Fig. 7. Immunohistological characterizations of chronically implanted *ki*-MEAs. **a**, Immunohistochemical staining images of horizontal brain slices after 8-week implantation of *ki*-MEAs. The experiments were conducted on 3 mice. 30-μm-thick slices were labeled for neurons (NeuN, green) and astrocytes [glial fibrillary acidic protein (GFAP), red]. Scale bars, 200 μm. **b**, Normalized fluorescence intensity of NeuN and GFAP as a dependence of distance from the edges of implanted threads (Mean±SD, n = 3 mice).

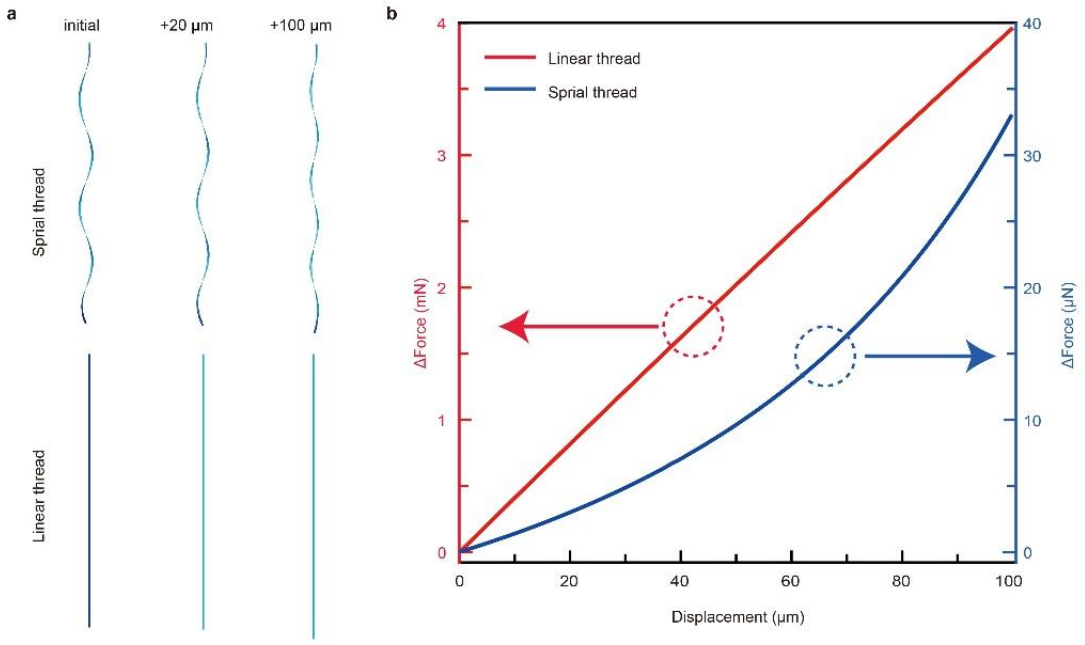

Supplementary Fig. 8. FEA simulation of spiral and linear threads upon simulated brain deformations. a, Conformations of a spiral thread and a liner thread upon 20 μm and 100 μm displacements. For each thread, one end is fixed, and the displacement is along the longitudinal direction. The width and thickness of the threads are 20 μm and 2 μm, respectively. The simulated implantation depths of the threads are 3 mm. **b**, Force-displacement curves of the spiral thread (blue) and the linear thread (red), respectively. The force required to stretch a linear thread by 100 μm is 4 mN. In contrast, the force requires to stretch a spiral thread by 100 μm is only 33 μN, which is over 2 orders of magnitude smaller than that of the linear thread.

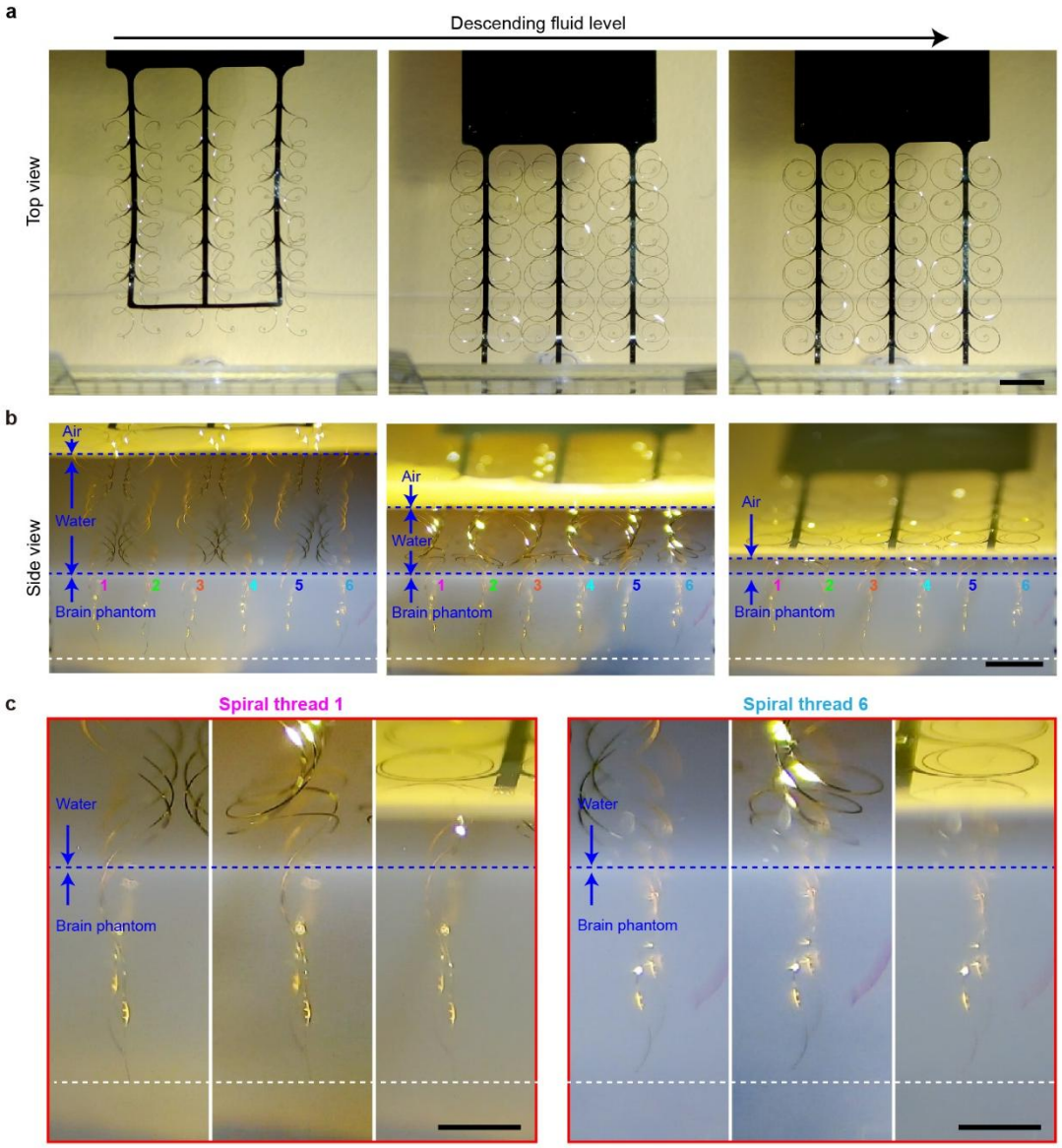

Supplementary Fig. 9. Floating design of *ki*-MEA. a, Top views of a 6X6 spiral thread array after implantation into an agarose brain phantom. Extra turns of spiral threads are left floating on the brain phantom after implantation. Scale bar, 2 mm. **b**, **c**, Side views of implanted spiral threads under fluctuations of fluid levels. The high stretchability of the floating spiral threads allows them to dynamically change their conformation to accommodate fluctuations of fluid levels. Consequently, the implantation depths of the spiral threads remain stable even in the presence of millimeter-scale fluctuations in fluid levels. Scale bars, 2 mm in **b** and 1mm in **c**.

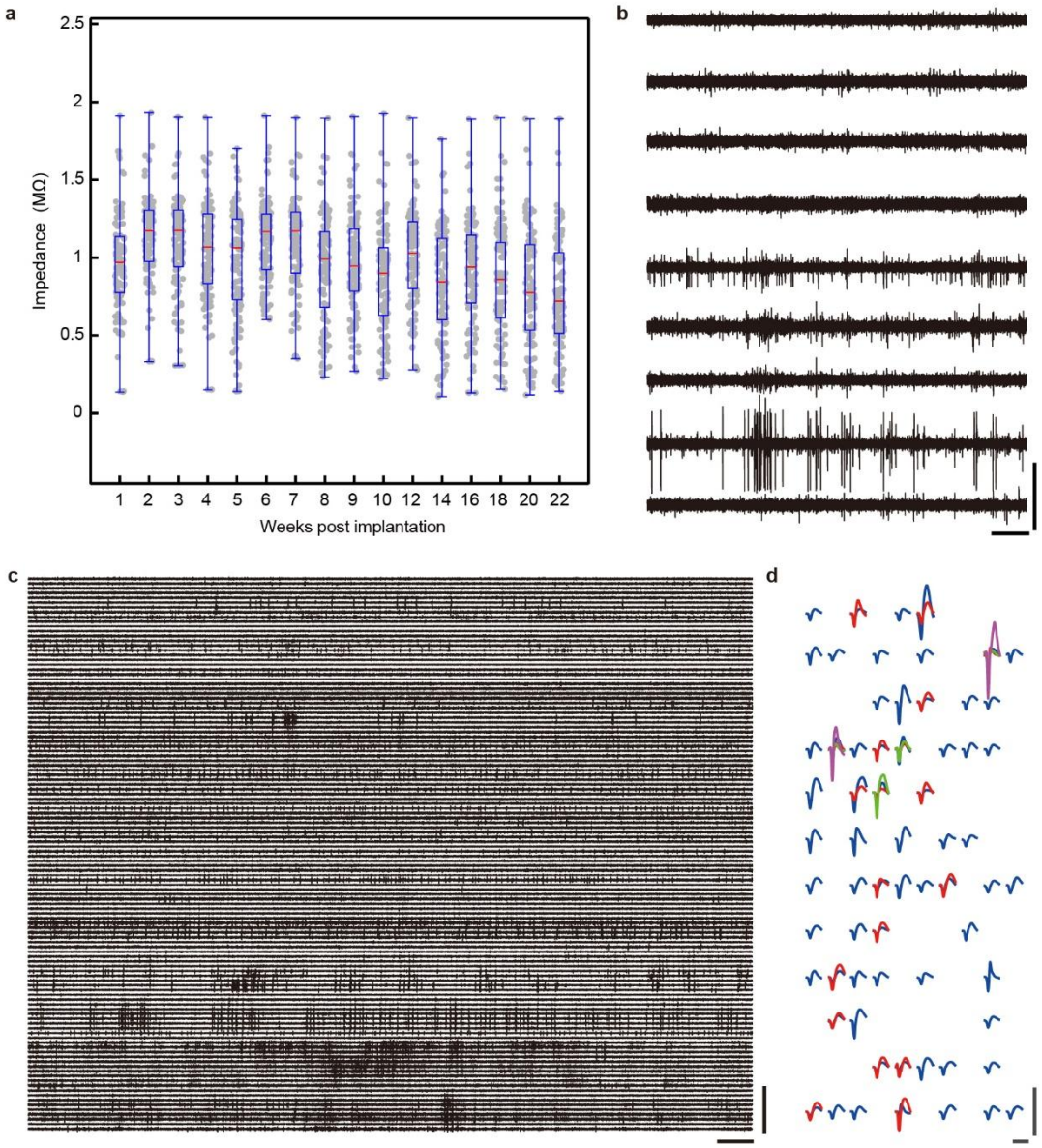

106

107 **Supplementary Fig. 10. Neuronal activity recordings by *ki*-MEA at 22 weeks post implantation**
108 **in macaque monkey brain. a**, Impedance of microelectrodes in the macaque monkey brain at 1-22
109 weeks post implantation. The impedance was measured at 1 kHz. All data points are represented by
110 grey dots, red lines indicated median, bottom and top box edges indicated percentiles of 25% (Q1) and
111 75% (Q3), whisker edges indicated min/max values respectively. **b**, Example raw action potential
112 traces recorded by a spiral thread (Spiral 4#) at 22 weeks post-implantation. Scale bars, 1 s (horizontal)
113 and 200 μV (vertical). **c**, Raw action potential traces recorded at 22 weeks post implantation. Scale
114 bars, 500 ms (horizontal) and 1 mV (vertical). The average noise level and signal-to-noise ratio at 22
115 weeks post implantation were 15±3 μV and 5.4±2.5, respectively. **d**, Waveforms of all recorded
116 neurons at 22 weeks post implantation. Scale bars, 1 ms (horizontal) and 200 μV (vertical).

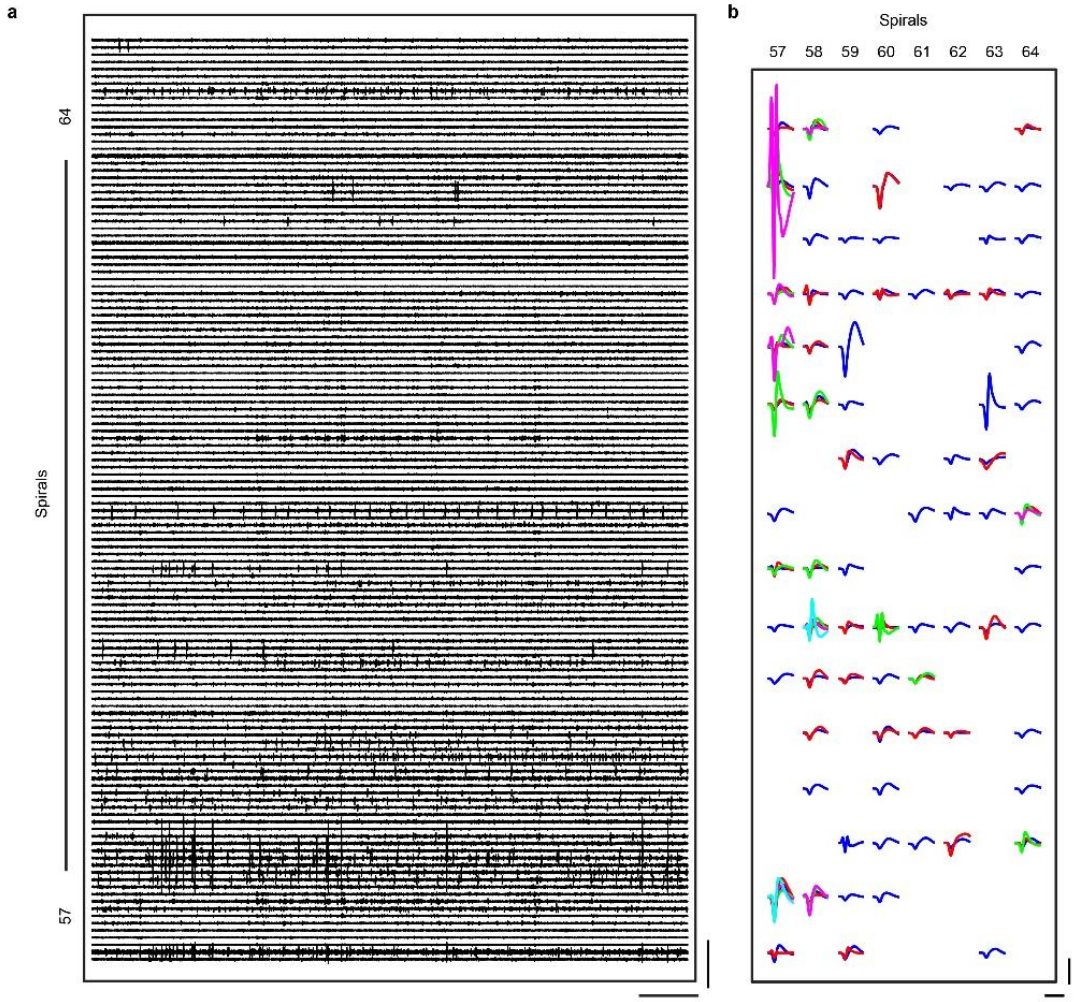

Supplementary Fig. 11. 1024-channle recording in monkey brain. a, Representative raw action potential traces recorded by Spiral 57-64. Scale bars, 1 mV (vertical) and 200 ms (horizontal). **b**, Representative waveforms of recorded neurons. Scale bars, 200 μV (vertical) and 1 ms (horizontal).

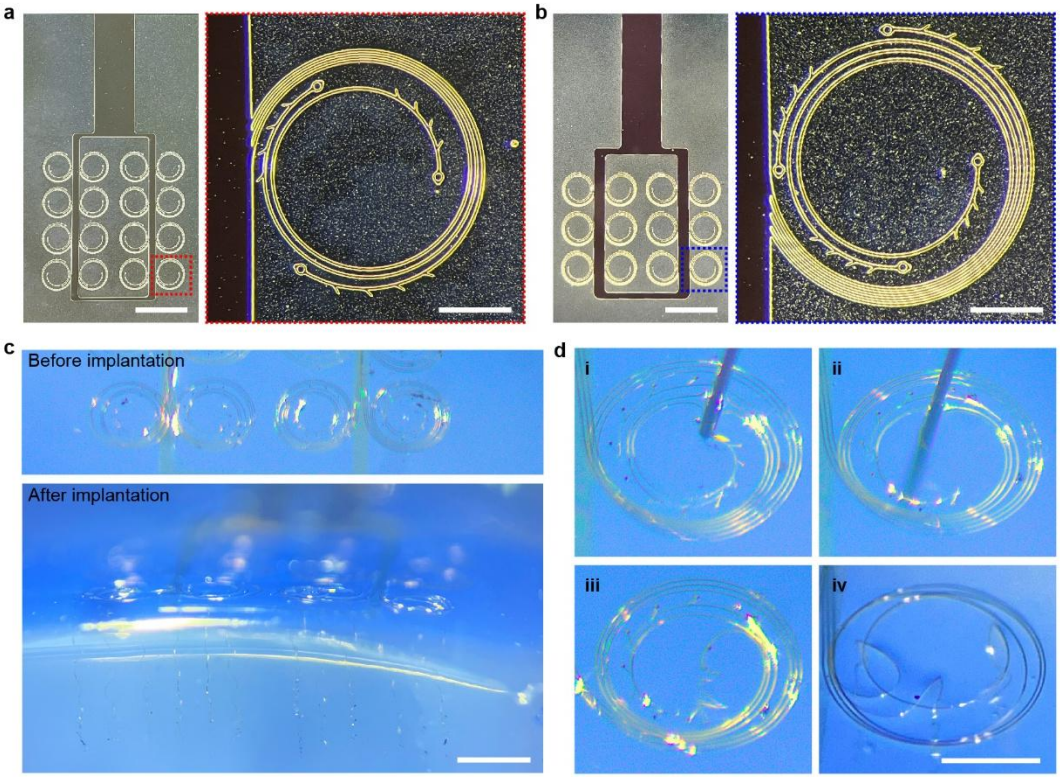

Supplementary Fig. 12. Structure and implantation of m-spiral thread arrays. a, Optical images of a three-spiral thread array. Each unit in the array consists of three parallel running spirals. Scale bars, 2 mm and 500 μm (enlarged image). **b**, Optical images of a four-spiral thread array. Each unit in the array consists of four parallel running spirals. Scale bars, 2 mm and 500 μm (enlarged image). **c**, Images of a three-spiral thread array before and after implantation into a brain phantom. Scale bar, 1 mm. **d**, Images of a three-spiral unit before and after implantation into a brain phantom. Scale bar, 500 μm.